Macromolecules

ARTICLE

pubs.acs.org/Macromolecules

Physics of Trapped Macromolecular Chains from Surface Force Apparatus Dynamic Measurements

Christophe Derail,*,† Fabrice Lapique,‡ and Jean-Pierre Montfort*,†

†Université de Pau et des Pays de l'Adour/CNRS IPREM UMR 5254, Equipe de Physique et Chimie des Polymères, 2 Avenue du Président Angot, 64053 Pau Cedex 09, France

‡SINTEF, Pb. 124 Blindern, NO-0314 Oslo, Norway

Supporting Information

ABSTRACT: We present experimental data of the rheological behavior of a polymer melt in a confined state. The polymer is adsorbed on the surfaces of the cell of a dynamic surface force apparatus. We analyze the variations of the zero-shear viscosity and the steady-state compliance with the separation of the surfaces by using a model of nonuniform medium. The viscosity of the adsorbed layers is about three times as much as in the melt, whereas their compliance increases by a factor of some thousands. Those results are described in terms of length distribution of the loops and tails and of their interconnection with the free chains. The impact of possible sliding motions either at the surfaces or between tethered and free chains is rejected in our experiment.

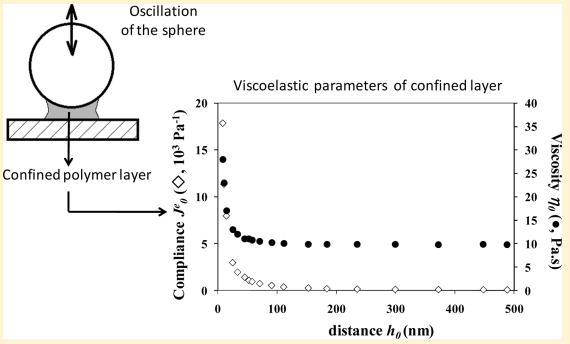

1. INTRODUCTION

As far as tethered macromolecular chains are concerned, many papers have been published which deal with their conformation,[1−3] their interconnection with free chains,[4−6] or the effect of confinement.[7,8] Some of them have been devoted to their response to mechanical stimulations: (i) exploration of the elasticity of individual chains trapped at both ends by using an atomic force microscope,[9−12] (ii) direct measurements of the interfacial velocity between anchored polymer chains and polymer melts by fluorescence recovery,[13] and (iii) investigation of the dynamics of macromolecular layers confined between two surfaces by using surface force apparatuses.[14−17]

The dynamic surface force apparatus (DSFA) enables the rheological properties of liquids to be studied at a length scale ranging from some nanometers to some micrometers. The harmonic force of interaction between the surfaces is a measure of the complex shear modulus $G^*(\omega)$ of the sample. Therefore, the viscoelastic behavior of solutions of polymer or polymer melts is investigated at a molecular scale.

Polymer solutions consist of polymer layers adsorbed to the surfaces and immersed in a solvent. As usual solvents are Newtonian liquids, the focus is mainly put on the effect of the overlap between the layers tethered to both surfaces. The behavior changes from being predominantly viscous at large distances to being predominantly elastic when the two layers overlap each other.[18,19] Both regimes were described theoretically[20] by using a Brinkman flow equation. A similar approach which uses a step-function concentration profile is suitable for grafted brushes in contact with a pure solvent.[21]

As far as polymer melts are concerned, the majority of the studies deal with unentangled polymers.[22,23] The adsorbed layers are separated by a viscous fluid made of similar chains. A viscous-elastic transition is observed from a distance of five to six times the unperturbed radius of gyration. A tentative explanation[22] combines an enhanced entanglement interaction to a slowing down of mobility near the surfaces. To our knowledge, very few works have been done with entangled adsorbed polymer layers.[24,25] The high level of forces exerted in the SFA by such samples needs to use a stiffer apparatus than the mica technique. The way to overcome that weakness of the traditional SFA has been to force the mica sheets to a parallel plate configuration and to perform friction experiments. Therefore, the separation range is restricted from contact to some radius of gyration.

In this paper, we are using a DSFA designed by Tonk et al.[26] and which is more effective for investigating the viscoelastic behavior of high molecular weight polymer melts. We restrict our study to nonoverlapped adsorbed layers separated by a melt of the same nature. In the first section, we present the experimental procedures and results. The second section is devoted to the analysis which is based on a description of the variation of the complex shear modulus with the distance to the surfaces in terms of a local complex shear compliance $J^*(\omega)$.[27]

2. EXPERIMENTAL SECTION

2.1. Description of the Experiments. We have used a surface force apparatus as a dynamic rheometer by applying an oscillating strain to the sample, which is confined between a plate and a sphere.

Received: April 19, 2011
Revised: July 29, 2011
Published: August 25, 2011

The sphere of radius R is vibrating in the vertical direction from a ground position at distance h_0 from the horizontal plate. The diameter of the sphere is equal to about 1 mm. The sphere and the plate were metalized with cobalt to permit conduction within the confined polymer sample and to obtain a negligible roughness for our measurements which has been evaluated by atomic force microscopy (AFM) below 1 nm rms.[20] The setup of the system is sketched in Figure 1.[26]

A drop of polymer is deposited onto the plate and confined between the plate and the sphere by an axial movement of the sphere imposed by a piezoelectric crystal. The hydrophobic surfaces of plate and sphere exhibit good wettability for polymeric samples. The sample is let overnight at large separation (some micrometers) for complete surface wetting and complete stress relaxation. The spring stiffness K allows us to measure the normal forces from 10^{-8} to 10^{-1} N. As the sphere and plate are made of glass and have been metalized, one can calculate the distance h_0 from the measurement of the capacitance formed by the plate-sphere capacitor. That distance h_0 can be compared to the distance H measured by the capacitance C_1. When the two surfaces are not deformed, the two distances exhibit the same variations. Furthermore, a distance-feedback loop incorporated into the C_1 circuit allows one to impose and control the plate-sphere distance. This last point is crucial for compensating all mechanical and thermal drifts. The normal forces were calculated from the deflection of the support of the plate which is measured precisely from the variation of the capacitance of the transducer C_2. The distance h_0 between the sphere and the plate will vary from about 10 nm to 10 μm. At each distance, the polymer is let until total relaxation of the sample (some hours, normal force returns to zero). The amplitude a of the sphere oscillation is of the order of 1 to 2 nm. We checked that the polymer was solicited in the linear domain by a strain sweep before the spectromechanical analysis. During the oscillation in the frequency range (10^{-3} and 10^{3} s^{-1}), the total normal force exerted on the plate can be analyzed in terms of in-phase and out-of-phase components by means of two lock-in amplifiers, and the sinusoidal shape of the signal is checked on the screen of an oscilloscope. The experiments have been conducted at room temperature. The plate-sphere separation depends strongly on temperature. Therefore, the DSFA has been confined in a homemade box which exhibits a temperature stability of about 0.01 °C at room temperature.

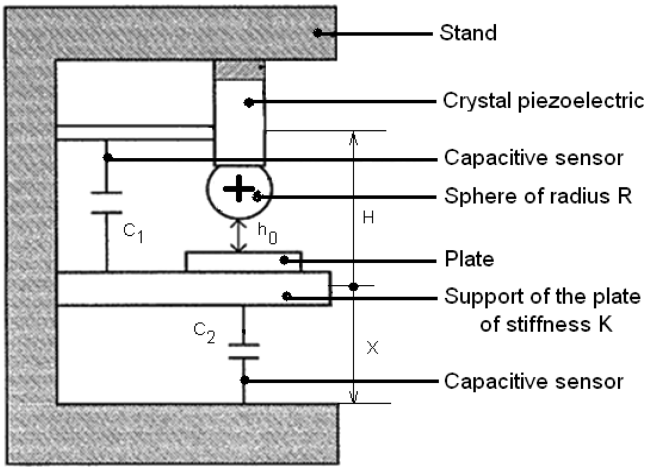

Figure 1. Mechanical description of the apparatus.

Chan and Horn expressed the lubrication force exerted by a fluid of viscosity η when the sphere is moved axially at velocity V in the case of no-slip conditions (eq 1).[28]

$$F(h_0) = -\frac{6\pi R^2 \eta V}{h_0} \quad (1)$$

For harmonic oscillations, Montfort et al. demonstrated that one can report the variation of the complex shear modulus as a function of frequency by measuring the force resulting from the vertical oscillation of the sphere.[17] For quasi-static vibrations of amplitude a ($a \ll h_0$) and frequency ω, the extension of eq 1 is given by eq 2 where F is the measured force, R the radius of the sphere, and G^* the complex shear modulus.

$$F^*(\omega, h_0) = -\frac{6\pi R^2 G^*(\omega, h_0) a}{h_0} \quad (2)$$

2.2. Polymer Characterization. We use a narrow entangled polybutadiene. Its main structural parameters are indicated in Table 1. The bulk complex shear modulus obtained on a classical dynamic rheometer and its evolution as a function of the separation h_0 measured with the DSFA are represented in Figure 2. The terminal viscoelastic parameters derived from the properties of the bulk are listed in Table 2.

Table 1. Parameters of the Polybutadiene Sample (PB10000)

molar mass M_w ($g \cdot mol^{-1}$)	dispersity I_p	molar mass between entanglements M_e ($g \cdot mol^{-1}$)	radius of gyration R_g (nm)
10 000	1.2	1800	3.8

Table 2. Bulk Viscoelastic Parameters of PB10000

zero-shear viscosity η_0 (Pa·s)	steady-state compliance J_e^0 (Pa^{-1})
9.8	10^{-6}

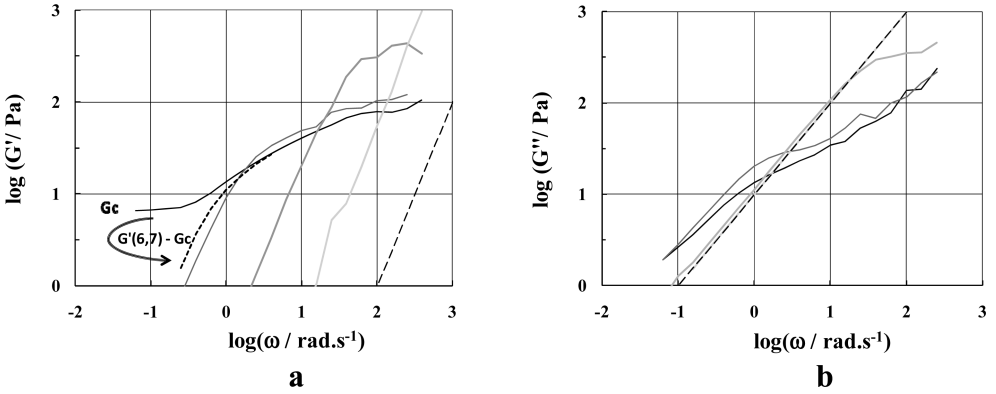

Figure 2. $\log(G')$ (a) and $\log(G'')$ (b) as a function of the logarithm of the circular frequency measured on the DSFA, $T = 20$ °C. Solid black line, 6.7 nm; black short dashed line, $G'(6.7) - G_c$; solid dark gray line, 89 nm; solid medium gray line, 371 nm; solid light gray line, 448 nm; black long dashed line, bulk.

dx.doi.org/10.1021/ma2009029 |Macromolecules 2011, 44, 7438–7444

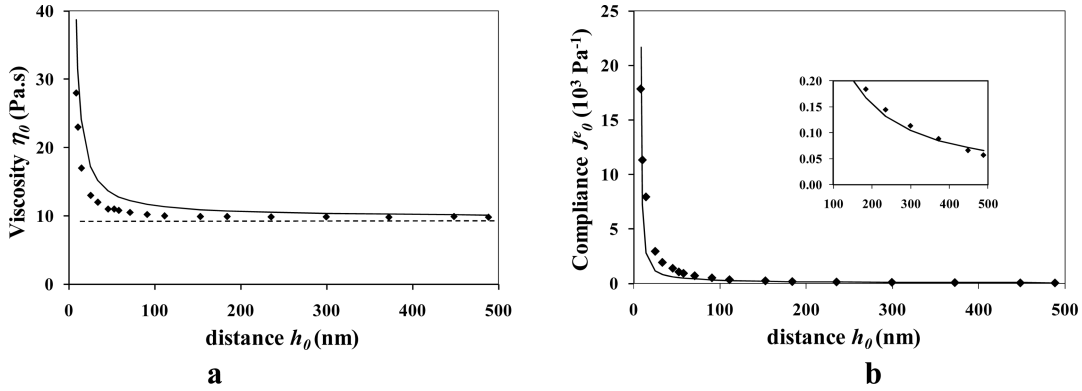

Figure 3. Experimental evolution of η_0 (a) and J_e^0 (b) as a function of h_0. The points are reported from the experimental data. The full lines correspond to the calculation explained in the last part.

2.3. Nanorheological Data. The complex modulus was measured at 18 different distances within the distance range explored and goes from 6.7 to 488.4 nm (±0.5 nm). Some viscoelastic data are reported in Figure 2. In the higher frequency domain, the transition toward the rubbery plateau is very different from one distance to another. The resolution of the apparatus do not allow us to perform reliable measurements for frequencies higher 100 s^{-1} for amplitudes soliciting the sample in the stress−strain linear domain. In the present paper, we will focus on the results obtained in the terminal zone. Each experiment covers this terminal zone of relaxation: slopes 2 and 1 are respected on $G'(\omega)$ and $G''(\omega)$, respectively.

We observe that the rheological behavior varies with h_0. The main trend is a shift of both curves toward low frequencies when the distance h_0 is decreasing. The shift of G' is more important than for G'' and begins at larger distances. From 488.4 to about 200 nm, G'' seems not to be affected by the decrease of the distance, and at the same time G' is shifted toward low frequencies when the two surfaces are closer. At some distance which can be related to the overlap of the layers of macromolecules trapped on both surfaces, the storage modulus shows a low frequency plateau G_c.[24] As that plateau modulus appears at a distance of about 8.6 nm, we attribute a value of 4.3 nm to the thickness e of each layer. It was shown that the storage modulus is the sum of a compression term G_c and of a shear modulus $G'-G_c$ (see Figure 2a for the distance equal to 6.7 nm). We are going to concentrate our study on distances higher than 2e.

In the terminal zone of the relaxation process, the complex shear modulus can be expressed as eq 3 where the zero-shear viscosity is noted η_0 and the steady-state compliance J_e^0. These global viscoelastic parameters depend on the separation h_0 between the two surfaces as shown in Figure 3.

$$G^*(\omega) = \omega^2\eta_0^2 J_e^0 + i\omega\eta_0 \tag{3}$$

The main feature is an increase of both parameters as the separation decreases but with different characteristics. The viscosity is steady from the bulk to about 200 nm and increases by a factor of about 3 when the adsorbed layers are beginning to overlap each other. At the same time, even at distances of the order of 100 times the thickness of each layer, that is, about 500 nm, the measured compliance is of the order of 5×10^{-5} Pa^{-1} which is 50 times higher than the bulk compliance. Moreover, at the overlapping threshold, the compliance is about three decades higher than at the largest separation. Then, the perturbation brought by the solid surfaces to the dynamics of free chains affects preferably the deformation properties. That peculiarity has already been observed for polydisperse melts where the viscosity is close to that of monodisperse samples of same average molecular weight whereas the compliance is much higher. In particular, in bimodal blends of monodisperse components, the increase of the compliance can reach three decades.[29] Such behavior is accounted for in the framework of the double reptation where each type of molecule is affected by the change of its own environment.[30] Within a surface force equipment, the melt is squeezed between two surfaces, and subsequently the adsorbed layers should not only exhibit different viscoelastic behavior as in free space but also modify that of the free molecules in contact with the layers. Could that correlation concern a thickness larger than some chain lengths, or is there any artifact occurring in the experiments?

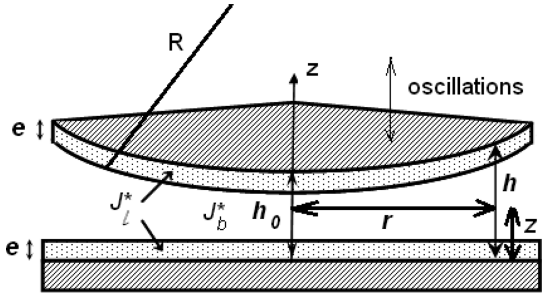

Figure 4. Scheme of the geometry of the cell. We have superimposed the three-layer description.

One artifact could be a sliding motion of the chains in contact with the surfaces. That point as been addressed by Vinogradova by introducing an extrapolation length b which is defined has the distance to the surface where the velocity is zero.[31] The consequence of that feature on the lubrication force is given in eq 4 for a viscous body and in eq 5 for a viscoelastic fluid.

$$F(R,h_0,b,V) = \frac{2\pi R^2\eta V}{b}\left[1-\left(1+\frac{h_0}{6b}\right)\ln\left(1+\frac{6b}{h_0}\right)\right] \tag{4}$$

$$F^*(\omega,h_0) = -\frac{6\pi R^2 G^*(\omega,h_0)a}{h_0} f(b/h_0) \quad \text{with} \quad f<1 \tag{5}$$

Therefore, in the presence of a sliding effect, the values of the calculated complex shear modulus according to eq 2 should be higher than the true values. That means that, according to eq 3, the measured viscosity should be higher and the compliance lower with the product $\eta_0 J_e^0$ constant. At large distances ($e \ll h_0$), we measure a compliance which is 50 times higher than the bulk value. The reciprocal does not occur for the viscosity which is the same as in bulk. That fact advocates for a nonsliding effect at the surfaces.

3. INTERPRETATION

3.1. Framework of the Analysis. Now, we are going to use a nonuniform description of the dynamics of a viscoelastic liquid trapped between a plane and a sphere (Figure 4).[27]

We recall that, when $h_0 \ll R$, the gap h at distance r from the z-axis is expressed by eq 6.

$$h = h_0 + \frac{r^2}{2R} \tag{6}$$

The general form of the complex shear modulus is given by eqs 7 and 8. $G^*(\omega,h)$ is the shear modulus integrated over the gap h at distance r from the axis. It is calculated from the local complex compliance $J^*(\omega,z)$ (eq 9). That semilocal modulus and its reciprocal $J^*(\omega,h)$ can be deduced from the measured modulus $G^*(\omega,h_0)$ by applying a double derivation to eq 7 and given eq 10.

$$G^*(\omega,h_0) = \frac{h_0}{3}\int_{h_0}^{\infty} \mathrm{d}h \int_h^{\infty} \frac{\mathrm{d}h}{\int_0^h \mathrm{d}z \int_0^z (h-2z)J^*(\omega,z)\,\mathrm{d}z} \tag{7}$$

$$G^*(\omega,h_0) = 2h_0\int_{h_0}^{\infty} \mathrm{d}h \int_h^{\infty} \frac{G^*(\omega,h)\mathrm{d}h}{h^3} \tag{8}$$

$$\frac{1}{G^*(\omega,h)} = J^*(\omega,h) = \frac{6}{h^3}\int_0^h \mathrm{d}z \int_0^z (h-2z)J^*(\omega,z)\mathrm{d}z \tag{9}$$

$$G^*(\omega,h) = \frac{h^3}{2}\left[\frac{\partial^2}{\partial {h_0}^2}\left(\frac{G^*(\omega,h_0)}{h_0}\right)\right]_{h_0=h} \tag{10}$$

3.2. A Three-Layer Description. In a first step, we describe the gap between the two surfaces as a three-domain fluid made of two identical layers interacting with the substrate and separated by a melt of free chains. We assume the viscoelastic behavior of the free chains identical to that of a bulk melt (index b), and we deduce that of the adsorbed layer (index l) from the expression of the lubrication force for a nonuniform fluid.

Figure 4 sketches a symmetrical gap made of two identical adsorbed layers (thickness e and compliance J^*_l) separated by a melt of free chains (local thickness h-2e and compliance J^*_b). Therefore, eq 7 gives the following form of the semilocal compliance (eq 11).

$$h^3 J^*(\omega,h) = J^*_b(h-2e)^3 + J^*_l[8e^3 - 12e^2h + 6eh^2] \tag{11}$$

Combining eqs 10 and 11, we end up with the expression of the semilocal compliance of the layers given by eq 12. In the terminal zone, the complex compliance can be written as proposed in eq 13 which allows us to calculate the steady-state compliance $J_l(h)$ and the zero-shear viscosity $\eta_l(h)$ within the layers. The bulk values for free chains are the same as the bulk values reported in the Table 2 ($J_b = 10^{-6}$ Pa^{-1} and $\eta_b = 9.8$ Pa·s). We recall that the thickness of the layers is evaluated at about 4.3 nm from the distance at which appears a steady value of G' at low frequencies accounting for the onset of the overlapping of the adsorbed chains.

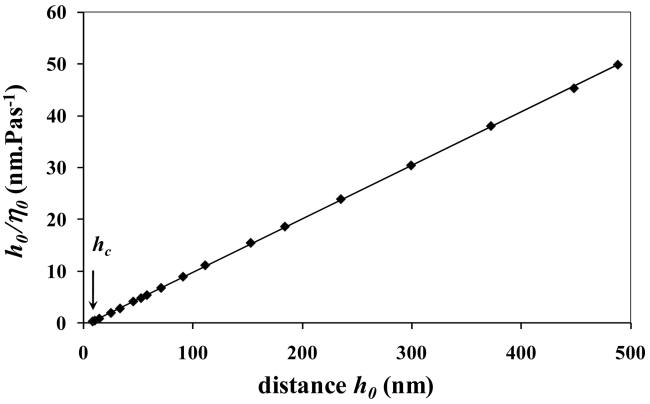

Figure 5. h_0/η_0 as a function of the distance h_0.

$$J^*_l(\omega,h) = \frac{\left[\frac{\partial^2}{\partial {h_0}^2}\left(\frac{G^*}{h_0}\right)\right]^{-1}_{h_0=h} - \frac{1}{2}J^*_b(h-2e)^3}{4e^3 - 6e^2h + 3eh^2} \tag{12}$$

$$J^* = J - \frac{i}{\omega\eta} \tag{13}$$

To calculate the second derivative of $G^*(\omega,h_0)/h_0$ in the terminal zone, we fit the experimental data of $\eta_0^2 J_e^0/h_0$ and of η_0/h_0 by a function where the viscoelastic parameters tend to their bulk values at large distances. We chose the form expressed by eq 14, where $a^*_1 = G^*_b$ and h_c stands for a distance at which the viscosity would be infinity (solid state response). One term is sufficient for fitting the experimental viscosity as the factor h_0/η_0 is a linear function of the distance as shown in Figure 5. The fitting function is given by eq 15. For G'/h_0, a good fit is obtained with the expression reported in eq 16. The fit is represented in Figure 6 by the bold curves. The value of h_c is lower than twice the thickness of each layer. Therefore, a solid state response of the polymer could start when the two layers are well-overlapped. The dashed lines represent the behavior of a homogeneous fluid with the bulk values at all distances. They confirm the strong increase of the compliance, even at large distances.

$$\frac{G^*}{h_0} = \sum_{i=1}^{3} \frac{a^*_i}{(h_0 - h_c)^i} \tag{14}$$

$$\frac{\eta_0(h_0)}{h_0} = \frac{9.71}{h_0 - 5.74} \tag{15}$$

$$\frac{\eta_0^2 J_e^0}{h_0} = \frac{10^{-4}}{h_0 - 5.74} + \frac{2.68}{(h_0 - 5.74)^2} + \frac{108}{(h_0 - 5.74)^3} - \frac{227}{(h_0 - 5.74)^4} \tag{16}$$

Then, we evaluate the local viscoelastic parameters of the layers at distance r from the z-axis with eq 11. Due to the simplified form of the variation of the viscosity (eq 15), the expression of the viscosity of the layers takes the form reported in eq 17. The expression of the layer compliance is more complicated as, when $\omega \to 0$, the real part of the reciprocal of the second derivative of

dx.doi.org/10.1021/ma2009029 |Macromolecules 2011, 44, 7438–7444

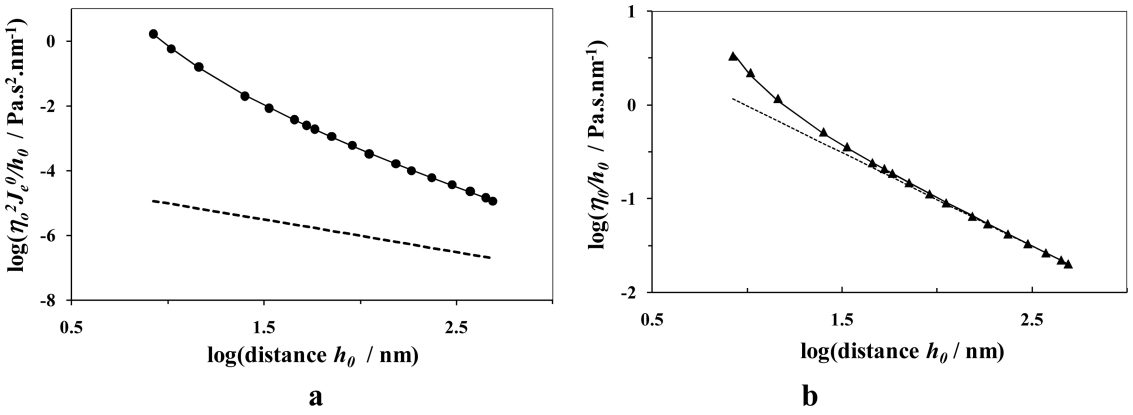

Figure 6. $\log((\eta_0^2 J_e^0)/h_0)$ (a) and $\log(\eta_0/h_0)$ (b) as a function of the logarithm of the distance h_0.

G^*/h_0 takes the form of eq 18.

$$\eta_l(h) = \eta_b \frac{6eh^2 - 12e^2h + 8e^3}{(h - h_c)^3 - (h - 2e)^3} \tag{17}$$

$$\text{real}\left[\frac{\partial^2}{\partial h_0^2}\left(\frac{G^*}{h_0}\right)\right]^{-1}_{h_0=h} = \left[\frac{\partial^2}{\partial {h_0}^2}\left(\frac{\eta_0^2 J_e^0}{h_0}\right)\right]_{h_0=h} \Big/ \left[\frac{\partial^2}{\partial {h_0}^2}\left(\frac{\eta_0}{h_0}\right)\right]^2_{h_0=h} \tag{18}$$

The variations of J_l and η_l with the confinement are shown in Figure 7 for a layer thickness e = 4.3 nm. The curves represent the entire range of variation of the viscoelastic parameters of the adsorbed layers as a function of the local distance h whatever the sphere-plate separation h_0. For a given separation, the confinement window is limited to values of h higher than h_0 as shown in Figure 1 of the Supporting Information.

At large distances, the viscosity of the layers levels off with a value of the order of 30 Pa·s which is three times higher than that of the free chains. It represents the viscosity of tethered chains but not confined and accounts for the intensity of the interaction with the substrate. The adsorbed chains do not see the other surface at distances higher than about 200 nm or a ratio h/e of about 50. At shorter distances, the viscosity within the layers shows some increase of about 50%. The variation of the compliance is somewhat different. It does not show any asymptotic behavior at large distances, and the values are more than 1000 times higher than for free chains.

The adsorbed chains consist of tails, loops, and trains. The trains are made of the monomers in direct interaction with the surface. The length distribution of the loops has been modeled by mean-field and scaling theories. For irreversibly adsorbed chains in presence of a melt, a scaling approach predicts a loop density profile $S(n) \cong an^{-1/2}$ where a is the monomer size and n the number of monomers.[32] Therefore an adsorbed chain can be seen as a star macromolecule with a broad distribution of arms (loops and tails). The high values of compliance come both from the dynamics of star arms—exponential variation with the length—and from the dispersity. We have already mentioned the effect of a broad length distribution in part II-3. It is dominant for the compliance and negligible for the viscosity. The viscosity is driven by the monomeric friction coefficient and an average length (or molecular weight). The compliance is related to the deformability of the chains which is more affected by the details

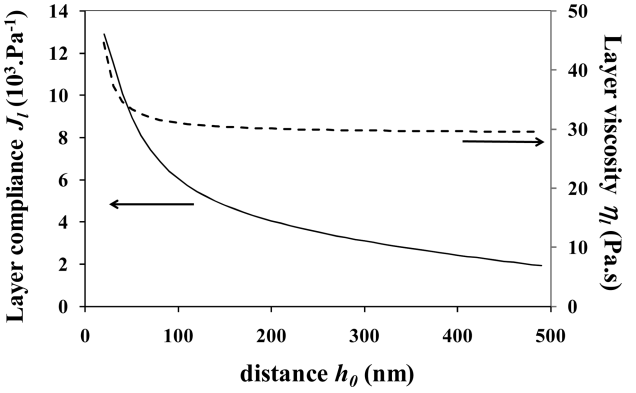

Figure 7. Compliance (left) and viscosity (right) of the layer as a function of the distance.

of their morphology and of the intermolecular interactions. Among them, the penetration of the free chains within the layers has to be considered. As the separation decreases, we assume that the monomer concentration profile within the layers is modified by the interaction with the free chains. Under this consideration, the dense short loops contribution is increasing, and the interpenetration between long loops, tails, and free chains leads to a broadening of the relaxation times distribution. At short distances, we cannot depict any more the central part of the gap as made of free chains but rather as a mixture of loops, tails, and free chains.

Another explanation for the high value of the compliance of the layers could be uncorrelated motions of the trains on the substrate. The center of the chain does not move in the time scale of those localized motions which modify the length distribution of the loops. Therefore, the main effect will be on the deformability of the adsorbed chains which is accounted for by the compliance.

The mechanisms which could be responsible for the high level of the steady-state compliance—length distribution of loops and tails, local and uncorrelated motions of trains—are difficult to quantify. A more comfortable situation is represented by end-grafted chains. Controlled radical polymerization allows one to obtain layers with well-defined thickness and grafting density.[33] The regimes of penetration of the brushes by a melt of the same chemical species have been studied both experimentally and theoretically.[6,34,35] They show that, as the surface coverage and melt chain length increase, the mobile chains are expelled from the brush.

dx.doi.org/10.1021/ma2009029 |Macromolecules 2011, 44, 7438–7444

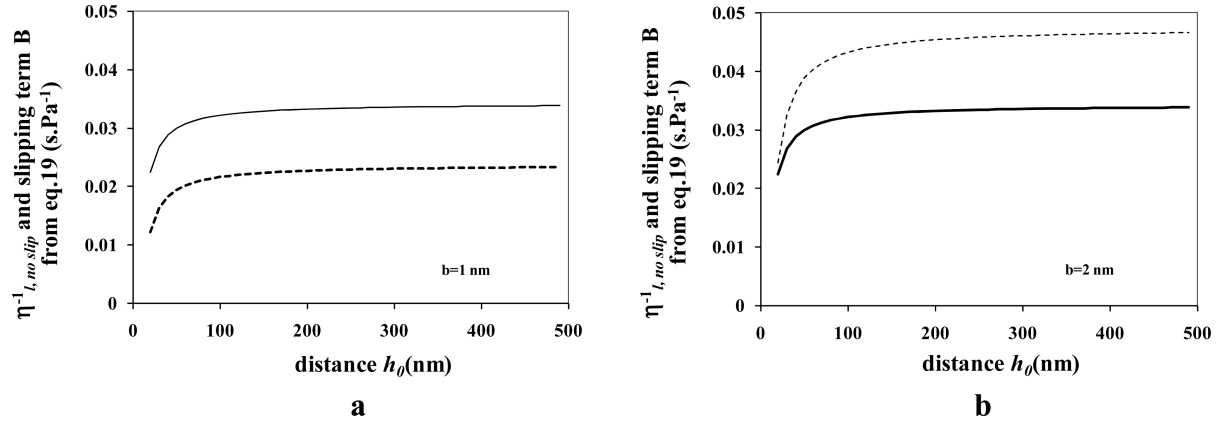

Figure 8. Slipping effect at the interface for two extrapolation lengths. For b = 1 nm (a), the viscosity of the layers would be three times as much as in absence of slipping. For b = 2 nm (b), the viscosity of the layers should be negative (solid lin, $1/\eta_l$; dashed line, term B).

At high surface coverage, the interaction between tethered and free chains is weak. During a shear experiment, a slipping motion is expected at the interface between grafted and free chains. Should such a motion occur between adsorbed and free chains?

3.3. Slippage at the Interface. We established the expression of the semilocal compliance $J^*(\omega,h)$ of a three-layer gap with slipping between the layers, in terms of compliance of adsorbed chains J^*_b compliance of the melt J^*_f, and extrapolation length b.[19] We recall the expression in eq 19.

$$h^3J^*(\omega,e,b,h) = J^*_b[(h-2e)^3 + 6b(h-2e)^2] + J^*_l[8e^3 - 12e^2h + 6eh^2] \quad (19)$$

It is worth noting that, for a homogeneous melt, $J^*_b = J^*_l$ and $e = 0$. Using the above expression of $J^*(\omega,h)$ in eq 6 with $e \to 0$ leads to the same slipping function $f(b/h_0)$ as in eq 4, we deduce the eq 20 of the compliance of adsorbed chains which can be compared to eq 12 without slipping (eq 21).

$$J^*_l(\omega,h) = \frac{\left[\frac{\partial^2}{\partial h^2}\left(\frac{G^*}{h_0}\right)\right]^{-1}_{h_0=h} - \frac{1}{2}J^*_b[(h-2e)^3 + 6b(h-2e)^2]}{4e^3 - 6e^2h + 3eh^2} \quad (20)$$

$$J^*_{l,\,\mathrm{slip}} = J^*_{l,\,\mathrm{noslip}} - 3J^*_b b\frac{(h-2e)^2}{4e^3 - 6e^2h + 3eh^2} = J^*_{l,\,\mathrm{noslip}} - BJ^*_b \quad (21)$$

We evaluated the correction for two values of the extrapolation length b = 1 nm and b = 2 nm. For both values, the correcting term has no impact on the compliance (ratio of the order of 10^{-4}). Figure 8 shows the value of the added term $(3b(h-2e)^2/\eta_b(4e^3 - 6e^2h + 3eh^2)$ noted B in eq 21, compared to that of $\eta^{-1}_{l,\mathrm{noslip}}$ for two values of extrapolation length. For b = 1 nm, the viscosity of the adsorbed chains should be three times as much as evaluated in the absence of slipping. But for $b \geq 2$ nm, the correcting term exceeds the first one, which leads to a negative value of the viscosity of the layers. For all of these reasons, the hypothesis of a slipping plane at the interface between adsorbed and free chains can be rejected.

3.4. Three Layers and Two Interphases. The broad length distribution of loops and tails and the penetration of free chains within the adsorbed layers advocate for the definition of an interphase. Its thickness ε can be seen as the penetration length of the free chains. We can sketch the variation of the local compliance and viscosity throughout the gap in the following way (Figure 9).

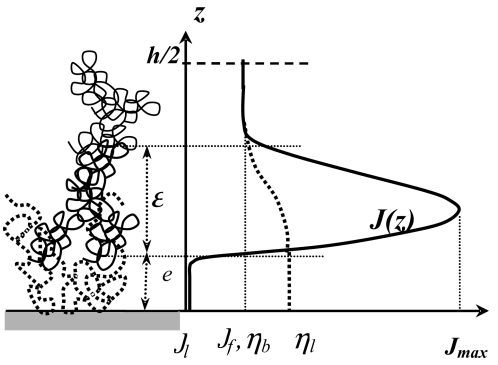

Figure 9. Variation of the local compliance and the viscosity throughout the gap between the sphere and the plane.

Within the overlapping zone, the viscosity is expected to vary steadily between two limits, η_l and η_b, whereas the compliance exhibits a maximum, accounting for the modification of the entanglement density. The thickness ε of the interphase can exceed a one-chain dimension as the overlap of free chains with tails and long loops will affect the dynamics of the adjacent free chains. ε plays the role of a correlation length between adsorbed and free chains. When the surfaces are separated by a distance h ranging from $2e$ to $2(e + \varepsilon)$, the symmetrical interphases overlap each other and reject free chains toward the outer part of the gap. In the Supporting Information, we propose an analytical expression which illustrates the variation of the local complex compliance throughout the gap at any separation h. Finally, the values for the overall viscoelastic parameters within the gap are calculated from eq 8 and plotted in Figure 3. The main trends of the variation of the viscoelastic properties are accounted for by such a description.

4. CONCLUSION

We conclude that a multiple-layer analysis could provide an interesting insight into the physics of trapped chains. The interactions with the surface modify at once the friction and

dx.doi.org/10.1021/ma2009029 |*Macromolecules* 2011, 44, 7438–7444

the deformation processes. The local friction is different for the segments close to the surface, those within the layer, and those belonging to the loop and tail ends. The viscosity which is related to an average friction coefficient within the layer cannot describe the details of the dynamics of the adsorbed chains. The viscosity of the tethered chains is higher than that of free chains which merely reveals the increase of the friction near attractive surfaces. At the contrary, the compliance is very sensitive to the details of the morphology of tethered chains. From the experimental data and a three-layer description, we have calculated that the compliance of the layers is two or 3 orders of magnitude higher than in bulk. We have attributed this result to the broad length distribution of the loops and to the interpenetration with free chains. We have shown that sliding motions either at the surface or between free and adsorbed chains are irrelevant with the observed behaviors. A quantitative analysis is difficult to conduct without mastering the structural parameters: interaction energy with the surface, length distribution function of the loops and tails, and penetration depth of the free chains within the layers.

A controlled situation is produced by layers of uniform end-grafted chains. Playing with the grafting density and the length of trapped and free chains should facilitate the interpretation of the observed behaviors. The picture of end-grafted chains as arms of star macromolecules will be more relevant. The chain ends are irreversibly attached to the surface. A narrow length distribution of the grafted chains conducts to a quite uniform layer thickness, the same for the penetration length of free chains.

We have focused our study on the terminal zone of the relaxation spectrum. It will be of interest to explore the entire range of frequencies encompassing the rubbery plateau region and the transition to the glassy domain. We have also limited our analysis to nonoverlapping adsorbed layers. For overlapped layers, the effect of the compression of the tethered chains should be considered.

■ ASSOCIATED CONTENT

Ⓢ Supporting Information. Local distance h for both geometries (Supporting Figure 1) and local complex compliance and viscosity profiles (Supporting Figure 2). This material is available free of charge via the Internet at http://pubs.acs.org.

■ AUTHOR INFORMATION

Corresponding Authors

*E-mail: christophe.derail@univ-pau.fr, jean-pierre.montfort@univ-pau.fr.

■ REFERENCES

(1) De Gennes, P. G. *Macromolecules* **1980**, *13* (5), 1069–1075.
(2) Scheutjens, J. M.; Fleer, G. J. *J. Chem. Phys.* **1980**, *84*, 178–190.
(3) Milner, S. T.; Witten, T. A.; Cates, M. E. *Macromolecules* **1988**, *21* (8), 2610–2619.
(4) Aubouy, M.; Fredrickson, G. H.; Pincus, P.; Raphaël, E. *Macromolecules* **1995**, *28* (8), 2979–2981.
(5) Aubouy, M.; Raphaël, E. *Macromolecules* **1994**, *27*, 5182–5186.
(6) Gay, C. *Macromolecules* **1997**, *30*, 5939–5943.
(7) Usatenko, Z. *J. Chem. Phys.* **2011**, *134*, No. 024119.
(8) Brochard, F.; de Gennes, P. G. *J. Chem. Phys.* **1977**, *67*, 52–56.
(9) Tranchida, D.; Sperotto, E.; Chateauminois, A.; Schönherr, H. *Macromolecules* **2011**, *44*, 368–374.
(10) Overney, R. M.; Leta, D. P.; Pictroski, C. F.; Rafailovich, M. H.; Liu, Y.; Quinn, J.; Overney, G. *Phys. Rev. Lett.* **1996**, *76* (8), 1272–1275.
(11) Kelley, T. W.; Schorr, P. A.; Johnson, K. D.; Tirrell, M.; Frisbie, C. D. *Macromolecules* **1998**, *31*, 4297–4300.
(12) Tranchida, D.; Piccarolo, S.; Loos, J.; Alexeev, A. *Macromolecules* **2007**, *40*, 1259–1267.
(13) Migler, K. B.; Hervet, H.; Leger, L. *Phys. Rev. Lett.* **1993**, *70*, 287–290.
(14) Granick, S.; Hu, H. W. *Langmuir* **1994**, *10*, 3857–3866.
(15) Israelachvili, J. N. *J. Colloid Interface Sci.* **1986**, *110*, 263–271.
(16) Klein, J. *Colloids Surf., A: Physicochem. Eng.* **1994**, *86*, 63–76.
(17) Montfort, J. P.; Hadziioannou, G. *J. Chem. Phys.* **1988**, *88*, 7187–7196.
(18) Luckham, P. F.; Manimaaran, S. *Macromolecules* **1997**, *30*, 5025–5033.
(19) Marr, J.; Hair, M. L. *Colloids Surf.* **1989**, *34*, 215–226.
(20) Sens, P.; Marques, M.; Joanny, J. F. *Macromolecules* **1994**, *27*, 3812–3820.
(21) Fredrickson, G. H.; Pincus, P. *Langmuir* **1991**, *7*, 786–795.
(22) Hu, H. W.; Granick, S. *Science* **1992**, *258*, 1339–1342.
(23) Israelachvili, J. N.; Kott, S. J.; Fetters, L. J. *J. Polym. Sci., Part B* **1989**, *27*, 489–502.
(24) Pelletier, E.; Montfort, J. P.; Loubet, J. L.; Tonck, A.; Georges, J. M. *Macromolecules* **1995**, *28*, 1990–1995.
(25) Pelletier, E.; Montfort, J. P.; Loubet, J. L.; Tonck, A.; Georges, J. M. *J. Polym. Sci., Part B* **1995**, *34*, 93–102.
(26) Tonk, A.; Georges, J. M.; Loubet, J. L. *J. Colloid Interface Sci.* **1988**, *126*, 150–163.
(27) Montfort, J. P. *Macromolecules* **2008**, *41*, 5024–5032.
(28) Chan, D. Y. C.; Horn, R. G. J. *J. Chem. Phys.* **1986**, *83*, 5311–5324.
(29) Montfort, J. P.; Marin, G.; Monge, P. *Macromolecules* **1984**, *17*, 1551–1560.
(30) des Cloiseaux, J. *Europhys. Lett.* **1988**, *5*, 437–442.
(31) Vinogradova, O. I. *Colloid J.* **1996**, *5*, 557–560.
(32) Guiselin, O. *Europhys. Lett.* **1992**, *17*, 225–230.
(33) Parvole, J.; Billon, L.; Montfort, J. P. *Polym. Int.* **2002**, *51*, 1111–1116. Parvole, J.; Laruelle, G.; Guimon, C.; Francois, J.; Billon, L. *Macromol. Rapid Commun.* **2003**, *24*, 1074–1078. Parvole, J.; Montfort, J. P.; Billon, L. *Macromol. Chem. Phys.* **2004**, *205*, 1369–1378.
(34) Hoy, R. S.; Grest, G. S. *Macromolecules* **2007**, *40*, 8389–8395.
(35) Mazzolin, C.; Auroy, P.; Deruelle, M.; Faulkers, J. P.; Leger, L.; Menelle, A. *Macromolecules* **2001**, *34*, 8694–8700.